Isolation and Characterization of the B-Cell Marker CD20

ARTICLE *in* BIOCHEMISTRY · DECEMBER 2005

Impact Factor: 3.02 · DOI: 10.1021/bi0511078 · Source: PubMed

Isolation and Characterization of the B-Cell Marker CD20

James A. Ernst,*[,‡,§] Hong Li,[‡] Hok Seon Kim,[||] Gerald R. Nakamura,[§,⊥] Daniel G. Yansura,[||] and Richard L. Vandlen[‡]

Department of Protein Chemistry, MS 63, Genentech, Inc., 1 DNA Way, South San Francisco, California 94080

Received June 9, 2005; Revised Manuscript Received August 30, 2005

ABSTRACT: The integral membrane protein CD20 has been identified as an important therapeutic target in the treatment of non-Hodgkin's lymphoma (NHL). CD20 binding of many antibodies including the therapeutic antibody, rituximab, has been shown to be critically dependent upon the conformation of a loop structure between the third and fourth helical transmembrane regions. In this work, human and murine CD20 proteins expressed in *Escherichia coli* are shown to be localized with the cell membrane and are purified in nondenaturing detergent solutions. The purified human and murine CD20 proteins have a substantial helical structure as measured by circular dichroism spectroscopy. Only small changes in the secondary structure are observed following the reduction of CD20, with the addition of SDS, or after heating. The rituximab antibody is shown to bind to purified human CD20 with nanomolar affinity. Rituximab binding is abolished by reduction and alkylation of CD20, with data consistent with the proposed antibody epitope being within the disulfide-bonded loop formed between cysteine residues 167 and 183. Disulfide-bond-dependent antibody binding is partially recovered following reoxidation of reduced CD20. Antibody binding is unaffected by mutations of cysteines proposed to be in the intracellular domain of CD20. The affinities of intact rituximab and its Fab fragment to the isolated and purified CD20 are similar to the observed affinity of rituximab Fab for CD20 on the surface of B cells. However, the intact rituximab antibody shows much higher affinity for CD20 on B cells. This suggests that B cells display CD20 in such a way that allows for marked avidity effects to be observed, perhaps through cross-linking of CD20 monomers into lipid rafts, which limits receptor diffusion in the membrane. Such cross-linking may play a role in partitioning CD20 into lipid rafts and in enhancing antibody-dependent B-cell depletion activities of rituximab and other therapeutic anti-CD20 antibodies.

The integral membrane protein CD20 was first identified as a marker for B cells over 20 years ago (*1*). It is expressed on pre-, naive, and mature B cells but not on plasma cells or early pro-B cells. It has further been established that this marker is present on the majority of B-cell lymphomas (*2*). Cloning of the gene for CD20 revealed an integral membrane protein with four transmembrane domains and a potential extracellular disulfide bond (*3*). CD20 has been shown to associate with MHC class II molecules by immunoprecipitation and fluorescence energy transfer (*4*, *5*) studies. In this regard, CD20 shows similarity to two other proteins, CD19 and CD21, which have been shown to interact with MHC class II complexes in B cells (*6*). However, at the primary sequence level, CD20 itself shows little sequence homology to CD19 and CD21, instead showing significant sequence homology to the high-affinity IgE receptor, hematopoietic cell-specific protein HTm4 (*7*), and the MS4A gene family of 16 tetra-spanning membrane proteins (*8*, *9*). Although no crystal structure of a tetra-spanning membrane protein is currently available, the proposed topology of CD20 is represented in Figure 1.

* To whom correspondence should be addressed. Telephone: (650) 225-5884. Fax: (650) 225-5945. E-mail: jernst@gene.com.

[‡] Department of Protein Chemistry.

[§] Department of Protein Engineering.

[||] Department of Molecular Biology.

[⊥] Department of Antibody Engineering.

Despite early progress, research on the function of CD20 has progressed slowly (*10*, *11*). However, the effectiveness of the recently introduced monoclonal antibody therapy (rituximab) in the treatment of non-Hodgkin's lymphoma (*12*) has renewed interest in the study of the gene and gene product. Recently, CD20 has been shown to specifically associate with lipid rafts in response to antibody binding (*13*). This relocalization appears to be enhanced by cross-linking with a subset of antibodies binding the extracellular loop of CD20 (*14*). Lipid raft association of CD20 may also be mediated in part by the intracellular region of CD20 because deletion of residues 219−225 reduced this localization effect (*15*).

Although CD20 does not share significant homology with any known ion channel, initial work on signaling of CD20 led to the hypothesis that CD20 might act as an ion channel to directly mediate cell signaling (*3*). Experiments demonstrating increased calcium conductance in transfected cells expressing CD20 supports a role for CD20 in regulating calcium conductance (*16*). More recently, siRNA experiments demonstrated reduced ion influx in B cells following reduced CD20 expression, potentially through a pathway involving the B-cell antigen receptor (BCR) and store-operated channels (SOCs) (*17*). Such experiments support a role for CD20 in the regulation of ion influx at channels. Interestingly, inhibiting the lipid raft association of CD20 also blocks the effects of CD20 on calcium SOC entry (*17*).

10.1021/bi0511078 CCC: $30.25
Published on Web 10/25/2005

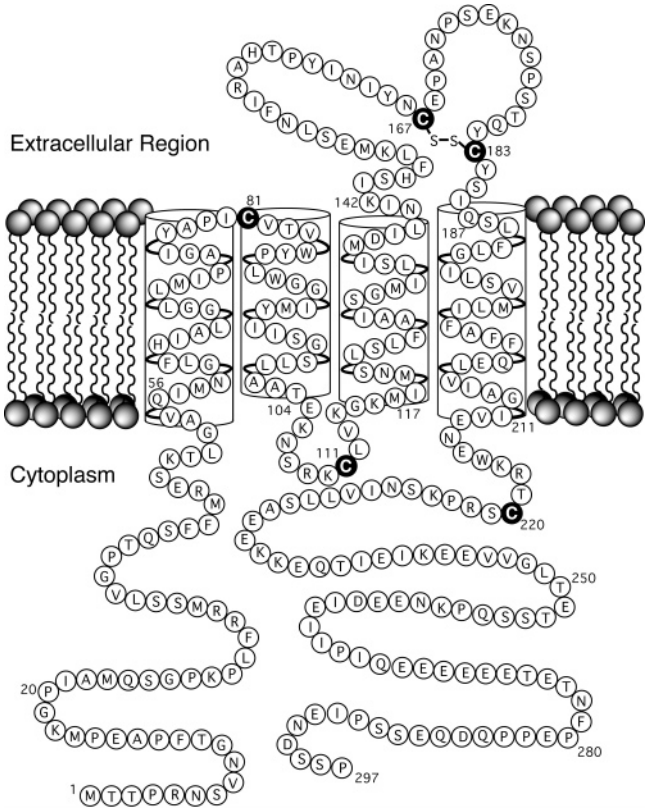

FIGURE 1: CD20 as presented on a B cell membrane. Sequence and proposed overall topology of CD20 as presented in the cell-surface membrane. Human and murine CD20 share 72% identity over all and 63% identity in the large extracellular loop.

Although important advances have been made in understanding the biological functions of CD20, a significant hurdle has existed in the direct analysis of CD20 because purified recombinant or native protein was unavailable for study. We, therefore, undertook to address this problem by expressing the CD20 gene in bacterial cells and purifying the protein in sufficient quantities to allow for initial biophysical and structural studies.

MATERIALS AND METHODS

All detergents were obtained from Anatrace, Inc., Maumee, OH. Unless otherwise mentioned, all chemicals were obtained from Sigma−Aldrich, St. Louis, MO.

Cloning and Expression. The cDNA for human and murine CD20 was subcloned, using standard molecular biology techniques (*18*), into a pBR322-derived plasmid containing the β-lactamase gene and tRNA genes for three rare *Escherichia coli* codons (*argU*, *glyT*, and *pro2*). A short MKHQHQQ sequence was added to the N terminus of CD20 to ensure high translation initiation, and an octa-His sequence was placed at the C terminus to aid in detection and purification. Gene transcription was under control of the *phoA* promoter. Gene expression was induced by dilution of a saturated LB carbenicillin culture into C. R. A. P. phosphate-limiting media (*19*). The culture was then grown at 30 °C for 24 h. Cysteine residues 111 and 220 were mutated to serines by site-directed mutagenesis to improve protein behavior (C2S mutant). Fermentor expression of CD20 was performed by the Genentech Process Sciences group (D. Reilly) (*19*).

Protein Purification. To determine detergent extraction conditions for the His-tagged human CD20 expressed in *E. coli*, 5 g of cells were resuspended using a Polytron (Brinkmann, Westbury, NY) in 50 mL of buffer A (20 mM Tris at pH 8.0 and 5 mM EDTA) and centrifuged at 12000*g* for 30 min. The cell pellet was then resuspended in buffer A, lysed by cell disruption using a microfluidizer (Microfluidics Corp., Newton, MA), and centrifuged at 125000*g* for 1 h. The pellet was washed once in the same buffer without EDTA and pelleted as before. The pellet was resuspended in 20 mL of buffer B (20 mM Tris at pH 7.5 and 300 mM NaCl) and aliquoted. Detergents were added to individual aliquots at the following concentrations: 1% SDS, 1% *n*-dodecyl-*N*,*N*-dimethylamine-*N*-oxide (LDAO), 1% dodecylphosphocholine (DDPC, Fos-Choline 12), 1% *n*-dodecyl-β-D-maltoside (DDM), 1% Triton-X 100, and 2.5% CHAPS. Pellets were extracted overnight at 4 °C, except for the SDS sample, which was extracted at room temperature. The following day, the samples were centrifuged and the supernatants were removed. Pellets and supernatants were resuspended in reducing SDS loading buffer to equal volumes and analyzed by SDS−PAGE followed by immunoblots on nitrocellulose membranes probed with horseradish-peroxidase-conjugated anti-His antibodies (Roche Applied Science, Indianapolis, IN).

For large-scale extraction, 100−200 g of cells were lysed and the insoluble fraction was prepared as previously described. To extract CD20 from the insoluble fraction, the final pellet was resuspended in buffer B at approximately 1:2.5 wt/vol from the starting wet cell weight, DDPC was added to 1%, and the solution was stirred overnight at 4 °C. The next day, the detergent-insoluble fraction was pelleted by ultracentrifugation at 125000*g* for 1 h. The supernatant was loaded onto a Ni-NTA Superflow (Qiagen, Inc., Valencia, CA) column pre-equilibrated in buffer C (20 mM Tris at pH 7.5, 300 mM NaCl, and 5 mM DDPC). The column was washed with 10 CV of buffer C with 20 mM imidazole and eluted with buffer C with 250 mM imidazole. All purification steps through column loading were performed at 4 °C.

Eluant fractions containing CD20 were concentrated and loaded onto a Superdex 200 column (Amersham Biosciences, Piscataway, NJ) pre-equilibrated in buffer C. The His-tagged wild-type human CD20 and murine CD20 were further purified over a 5 mL HiTrap HP Q (Amersham Biosciences, Piscataway, NJ) column prior to gel filtration.

For detergent exchange, samples were passed over a Superdex 200 column in buffer D (0.1% DDM, 150 mM NaCl, and 20 mM HEPES at pH 7.2). Alternatively, samples were bound to a small Ni-NTA column, washed with buffer B and detergent, and eluted in buffer B with detergent and 300 mM imidazole. These samples were then dialyzed against buffer B and detergent to remove imidazole.

For affinity purification of human CD20, rituximab was immobilized at 6 mg/mL on 10 mL of Actigel ALD Superflow resin (Sterogene, Carlsbad, CA). This resin was placed in a column and equilibrated in buffer D. Human CD20 C2S mutant, purified as previously described for native hCD20, was passed over the column, and the unbound protein was removed by extensive washing in buffer D. Protein was eluted in 0.1% DDM, 150 mM NaCl, and 20 mM sodium citrate at pH 3.5. Eluted samples were im-

mediately neutralized, concentrated, and dialyzed against buffer D. The protein concentration was determined by BCA (*20*) (Pierce Biotechnology, Rockford, IL), and samples were stored at −80 °C prior to use.

Full-length rituximab antibody was obtained from Genentech Manufacturing. Rituximab Fab was expressed in *E. coli* and purified by protein A and cation-exchange chromatography.

Density Gradient Centrifugation. A discontinuous sucrose gradient was generated by layering 1.9, 1.4, and 0.8 M sucrose solutions buffered with 150 mM NaCl and 20 mM HEPES at pH 7.2, in centrifuge tubes. Cells were lysed in buffer A containing 1 mM EDTA by cell disruption. The insoluble fraction was isolated by centrifugation at 38000*g* for 1 h. The supernatant was discarded, and the pellet was resuspended in the lysis buffer with the addition of 0.25 M sucrose at 1:5 wt/vol; 100 μL of this resuspension was mixed with 900 μL of the 1.9 M sucrose solution. The resulting mixture has a final concentration of 1.75 M sucrose. This mixture was then placed at the bottom of a centrifuge tube, and 1 mL of the 1.4 and 1.8 M sucrose solutions was layered above. A final 200 μL layer of the 0.25 M sucrose solution was then added to the top of the tubes. Samples were loaded into an SW55 rotor and spun for 1 h at 100000*g*. Samples were then carefully unloaded in 200 μL aliquots from the top of the tube, analyzed by SDS−PAGE, transferred to nitrocellulose, and probed with horseradish-peroxidase-conjugated anti-His antibody.

ELISA Assays. The 96-well plates were coated overnight at 4 °C with 100 μL of CD20 at 1 μg/mL in PBS with solubilizing detergent diluted to below its critical micelle concentration. Plates were then washed 3 times with PBS containing 0.05% Tween-20 (PBST) and blocked for 45 min at room temperature with 200 μL of PBST containing 0.5% BSA (blocking and assay buffer). Plates were again washed 3 times with PBST and probed with the primary antibody. A total of 150 μL of rituximab at 60 μg/mL in the assay buffer was added to the appropriate wells, and 3-fold serial dilutions were performed in the subsequent wells by taking 50 μL from the first well and mixing with 100 μL of the assay buffer in the next and subsequent wells to a final concentration of approximately 2 ng/mL. After 90 min of incubation at room temperature, the plates were washed with PBST and bound rituximab was detected with 100 μL of horseradish peroxidase conjugate goat anti-human F(ab′)2 (Jackson ImmunoResearch Laboratories, Inc., West Grove, PA) diluted 1:2000 in the assay buffer, washed 6 times with PBST, and developed with 100 μL/well of TMB Microwell Peroxidase Substrate System (KPL, Gaithersburg, MD) mixed according to the instructions of the manufacturer. The reaction was halted by the addition of 100 μL/well of 1.0 M phosphoric acid, and the absorbance was measured at 450 nm using a plate reader.

Reduced and alkylated CD20 samples were prepared by reduction with 10 mM DTT and alkylation by addition of 25 mM iodoacetamide. The reaction was halted by a further addition of 100 mM DTT. After each step, the reaction was allowed to proceed for 30−60 min at room temperature at pH 8.0. For reduction and reoxidation, the CD20 sample was reduced with 10 mM DTT prior to plating and allowed to reoxidize in the absence of DTT for several hours on the plate before antibody binding.

Table 1: IgG and Fab Binding to Isolated Human CD20[a]

	Rituximab Full-Length IgG[b]			
CD20 sample	$k_{on}/10^3$ (M^{-1} s^{-1})	$k_{off}/10^{-4}$ (s^{-1})	$K_a/10^6$ (M^{-1})	$K_d/10^{-9}$ (M)
CD20	2.5	4.1	6.6	160
C2S CD20	4.5	7.6	5.9	170
affinity-purified C2S CD20	8.7	7.3	12	84
	Rituximab Fab[c]			
CD20 sample	$k_{on}/10^3$ (M^{-1} s^{-1})	$k_{off}/10^{-4}$ (s^{-1})	$K_a/10^6$ (M^{-1})	$K_d/10^{-9}$ (M)
CD20	1.7	4.8	3.5	280
C2S CD20	4.9	11	4.4	230
affinity-purified C2S CD20	7.4	14	5.4	190

[a] Binding parameters of rituximab IgG or rituximab Fab to human CD20 His-tagged protein, C2S mutant of human CD20, and affinity-purified C2S CD20. [b] Binding to full-length rituximab. [c] Binding to rituximab Fab. Data are fit to a single binding site model. K_d and K_a values are calculated from association and dissociation rates.

Surface Plasmon Resonance. Rituximab affinities and binding kinetics for isolated human CD20 proteins were determined using a Biacore-3000 instrument (Biacore, Inc., Piscataway, NJ). A CM5 sensor chip was activated for covalent coupling of rituximab or rituximab Fab using *N*-ethyl-*N*′-(3-dimethylaminopropyl)-carbodiimide hydrochloride and *N*-hydroxysuccinimide according to the instructions of the supplier. Rituximab or rituximab Fab were diluted 5−10-fold to a concentration of 100 μg/mL in 10 mM sodium acetate at pH 5.0 and injected onto the activated chip. The remaining active coupling sites were blocked with 1 M ethanolamine. Intact rituximab was deposited at 8000−12 000 RU, and the rituximab Fab was deposited at 4000−7000 RU.

For kinetic measurements, seven 2-fold dilutions (a total of eight samples) of human CD20 from a starting concentration of 5 μM in 0.1% DDM, 150 mM NaCl, and 20 mM HEPES at pH 7.2 and 25 °C were injected with a flow rate of 30 μL/min for 100 s. Bound protein was allowed to dissociate for 720 s. At the end of each sample measurement, the sensor surfaces were regenerated by injecting 20 μL of 10 mM HCl. After sensograms were corrected for signals from a reference flow, kinetics were calculated using a simple 1:1 model with Biaevaluation 3.0 (Biacore) as shown in Table 1.

Circular Dichroism (CD). Detergent solutions of CD20 in either 0.1% DDPC or 0.1% DDM were prepared by dialysis against 100 mM sodium phosphate at pH 7.2 and either 0.1% DDPC or 0.1% DDM. CD data were collected using an AVIV202 instrument on 2−5 μM protein samples in a 1 mm quartz cuvette; wavelength scans were performed at 25 °C over the indicated regions in 2 nm increments with a 10 s averaging time. Data are plotted over the range from 185 to 285 nm, except for samples containing β-mercaptoethanol, for which data are truncated at 200 nm because β-mercaptoethanol interferes with data collection at lower wavelengths.

Scatchard Analysis of Rituximab IgG and Fab Binding to Normal Human B Cells. Equilibrium dissociation constants (K_d) were determined for rituximab IgG and rituximab Fab fragments for binding to B cells using radiolabeled protein. All dilutions were performed in binding assay buffer (DMEM media containing 0.5% bovine serum albumin, 25 mM

HEPES at pH 7.2, and 0.01% sodium azide). Aliquots (0.05 mL) of rituximab ^{125}I-IgG (iodinated with Iodogen) or ^{125}I-Fab (iodinated with Iodogen or lactoperoxidase) at a concentration of 0.005 or 0.05 nM, respectively, were dispensed into wells of a V-bottom 96-well microassay plate, and serial dilutions (0.05 mL) of cold antibody were added and mixed. Purified human B cells (125 000 in 0.05 mL) were then added. The plate was sealed, incubated at room temperature for 24 h, and then centrifuged for 15 min at 2500 rpm. The supernatant was aspirated, and the cell pellet was washed and centrifuged. The supernatant was again aspirated, and the pellets were dissolved in 1 N NaOH and transferred to tubes for γ counting. The data were used for Scatchard analysis (*21*) using the program Ligand (*22*).

Normal human B cells were isolated from 100 mL of heparinized normal human blood by negative selection using the RosetteSep B Cell Enrichment Cocktail (Stemcell Technologies, Vancouver, Canada) according to the protocol of the manufacturer. B cells were further separated over Ficoll-Paque (Amersham Biosciences, Peapack, NJ) and then isolated and washed in phosphate-buffered saline. Any remaining red cells were lysed by a 30 s exposure to a hypotonic solution. The purified B cells were then adjusted to a concentration of 1−2 million cells/mL in binding buffer.

RESULTS AND DISCUSSION

The primary structure of human CD20 is shown in Figure 1. The proposed topology of CD20 is that of a tetra-spanning membrane protein, with both termini in the cytoplasm. The two extracellular loops of CD20 are strikingly different in size. The first loop between helix one and helix two is extremely small and seems unlikely to protrude extensively from the membrane. The size of this loop is highly conserved in other members of the MS4A family (*8*, *9*). The second loop between helix three and helix four is approximately 46 amino acids in length extending from the region of residue 140 to the region of residue 185 and contains one possible disulfide bond between residues 167 and 183. The size of this loop varies widely among the amino acid sequences of the genes in the MS4A family, although most of these sequences retain the ability to form an extracellular disulfide bond (*8*, *9*). On the cytoplasmic side of the membrane in resting B cells, CD20 is phosphorylated (*23*), whereas phosphorylation is increased in response to antibody cross-linking (*24*). No other post-translational modifications have been identified on CD20, and the human protein lacks any consensus N-glycosylation sites in the extracellular region.

To ascertain the structure of CD20 and the potential role of disulfide bond formation in antibody binding, His-tagged human CD20 protein was expressed in *E. coli* as described. The potential for native expression of the protein in *E. coli* was evaluated by localizing the cellular expression of CD20 to the membrane by density gradient centrifugation and by testing protein solubility in native detergents.

Approximately half of the total protein expressed in bacteria was found to be localized with the bacterial membrane, migrating to a sucrose layer with a density less than 1.29 g/cm^2 (1.75 M sucrose) as shown in Figure 2a. Typical soluble proteins have a density of 1.33−1.42 g/cm^2 (*25*) and would be found at the bottom of the sucrose gradient, while membrane-bound proteins migrate to a lower

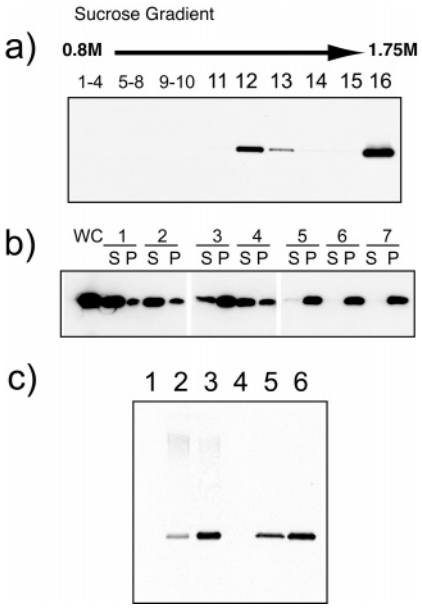

FIGURE 2: Localization and isolation of CD20. (a) Anti-His-tag Western blot of human His-tagged CD20 following sucrose gradient flotation. Sample fractions are indicated at the top of the gel. Samples from the fractions 1−4, 5−8, and 9−10 were pooled, and each pool was run in a single lane; samples from fractions 11−16 were run in individual lanes as indicated. An immunopositive band was isolated just after fraction 11, which corresponds to the transition from the 1.49−1.75 M sucrose layers. (b) Anti-His-tag Western blot of human His-tagged CD20 following detergent extraction from *E. coli* cell membranes. WC, whole cell extracts; S, supernatant; P, pellet; sample 1, SDS; sample 2, *n*-lauryl sarcosine; sample 3, LDAO; sample 4, DDPC; sample 5, DDM; sample 6, Triton-X 100; sample 7, CHAPS. Insoluble fractions of *E. coli* expressed His-tagged human CD20 were extracted with 1% of the indicated detergent. The samples were centrifuged; the pellets and supernatants were suspended in equal volumes of SDS buffer; and equal volumes of each were electrophoresed on SDS−PAGE under reducing conditions. For comparison, an equal volume of a whole cell (WC) fraction was suspended in SDS buffer after lysis but without any manipulation. (c) Anti-His-tag Western blot of *E. coli* cells expressing the His-tagged native and the C2S mutant of human CD20. Lane 1 and 4, control empty vector; lanes 2 and 5, His-tagged human CD20; lanes 3 and 6, C2S mutant human CD20. Samples in lanes 1−3 were run under nonreducing conditions; samples in lanes 4−6 were reduced with 100 mM DTT. Each lane contains equal volumes of cells normalized by optical density.

density because of the presence of lipid around the protein. These data are consistent with the localization of human CD20 to a cellular membrane fraction of the bacteria because *E. coli* membranes have a reported density of 1.15-1.25 g/cm^2 (*26*). These observations are similar to previous reports on the expression of other eukaryotic membrane proteins in a native conformation in the cellular membranes of bacteria (*27*, *28*).

Solubilization conditions for CD20 were determined by screening an array of nondenaturing and denaturing detergents (Figure 2b). A substantial fraction of CD20 was soluble in the nondenaturing zwitterionic detergent DDPC; thus, this detergent was selected for further work in extraction and purification of CD20.

Human CD20 was extracted from *E. coli* membranes with DDPC and purified by Ni^{2+} chelation using the C-terminal His tag. The addition of N- and C-terminal His tags to proteins has previously been shown to have a limited effect on the structures of both soluble and membrane-localized

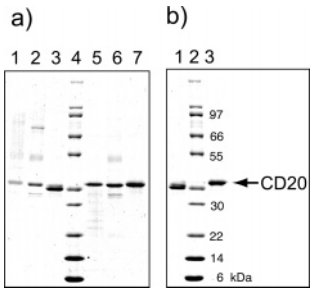

FIGURE 3: Purified His-tagged human CD20, C2S human CD20, and murine CD20. (a) Coomassie-stained SDS gel of purified CD20. Lane 1, human CD20 nonreduced; lane 2, C2S human CD20 nonreduced; lane 3, murine CD20 nonreduced; lane 4, Mark12 (Invitrogen) molecular-weight markers; lane 5, human CD20 reduced; lane 6, C2S human CD20 reduced; lane 7, murine CD20 reduced. Each lane contains 2 μg of protein. (b) Coomassie-stained SDS gel of purified murine CD20. Lane 1, 2 μg of murine CD20 nonreduced; lane 2, Mark12 molecular-weight markers; lane 3, 2 μg of murine CD20 reduced. Molecular weights of protein markers shown in a and b are 200, 116, 97, 66, 55, 36, 30, 22, 14, and 6 kDa.

proteins. The isolated protein was further purified using size-exclusion and anion-exchange chromatographies as described earlier. Approximately 10−20 μg of purified His-tagged CD20 protein were obtained from 1 g of bacterial cells.

Representative samples of purified His-tagged human CD20 are shown in the SDS polyacrylamide gel in Figure 3a (lanes 1 and 5). The protein migrates with an apparent molecular weight of approximately 38 kDa under reducing conditions, which is in reasonable agreement with the calculated molecular weight of 35 kDa.

Purified CD20 also shows a modest change in mobility under nonreducing and reducing conditions on SDS−PAGE. This can be clearly seen in Figure 3b, where reduced and nonreduced murine CD20 have been run in neighboring lanes for emphasis. This suggests that CD20 exists in a more compact, faster migrating structure because of the disulfide bond in the large extracellular loop, which is abolished upon addition of the reducing agent.

Although the nondenaturing detergents DDM and LDAO demonstrated only limited ability to solubilize CD20, large-scale purification was attempted with these reagents to assess if detergent solubilization from *E. coli* was indeed accurately quantitated by Western blots using the conditions described in Figure 2b. Protein purified using either DDM or LDAO was significantly less pure, and the procedures yielded significantly less protein than purifications performed with DDPC. However, CD20 could be successfully exchanged into nonionic detergents following purification, indicating that DDPC does not possess a unique ability to solubilize CD20.

We purified murine CD20 under similar conditions to those used to purify human CD20. Results of this purification are shown in Figure 3a (lanes 3 and 7). We noticed that this material was significantly better behaved than human CD20, showing less aggregation on nonreducing SDS gels (compare lanes 1 and 3 of Figure 3a) and providing a higher final protein yield. Inspection of the primary sequence of murine and human CD20 shows that cysteine residue 111 (Figure 1) in the human sequence is a serine in the murine protein; this implies that Cys 111 is not essential for the activity of CD20. Additionally, it has been shown that cysteine 220 may

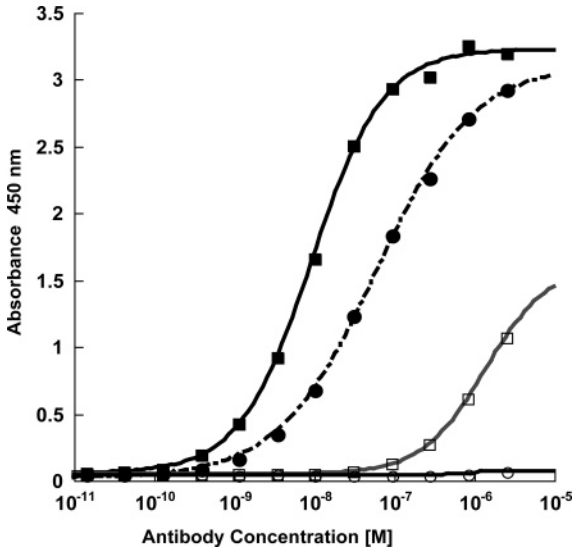

FIGURE 4: Disulfide-dependent antibody binding to His-tagged human CD20. Binding of rituximab to nonreduced CD20 (—, ■), CD20 reduced and alkylated (gray line, □), reduced CD20 that has been allowed to reoxidize (- - -, ●), and control (PBS) (—, ○). The curves for rituximab binding were determined from a four-parameter fit analysis.

not be essential because mutated human CD20 in which the cysteine at this location has been changed to alanine shows similar expression and antibody-dependent lipid raft association as compared to wild-type protein when expressed in eucaryotic cells (*15*). We, therefore, mutated both cysteine residues 111 and 220 in the human CD20 sequence to serine residues (C2S mutant) and expressed and purified this protein in a method similar to the His-tagged human CD20. As expected, these mutations of human CD20 showed improved protein behavior relative to the native protein. The C2S human CD20 was expressed at a higher level in *E. coli* and showed less disulfide-dependent aggregation (see Figure 2c). The purified protein, likewise, showed less aggregation (compare lanes 1 and 2 and 5 and 6 in Figure 3a) with an approximately 2-fold higher protein yield.

We next sought to assess whether purified, recombinant CD20 adopts a native conformation. To do this, we took advantage of the properties of the chimeric antibody rituximab. This antibody is known to bind to a structurally constrained extracellular loop of human CD20 expressed on the surface of B cells (*29*). An ELISA assay was developed on the basis of the binding of rituximab to purified human CD20. In this assay, rituximab binds His-tagged human CD20 with an EC_{50} of 9.4 nM as determined from a four-parameter fit of the data (see Figure 4). Rituximab binding has been localized to the extracellular loop of CD20 between residues K142 and Y184 (*29*). Two residues in this region C167 and C183 are thought to form a disulfide bond (*3*). Rituximab binding, in turn, is thought to be critically dependent upon the presence of this disulfide bond. To evaluate the importance of this disulfide bond in CD20 for the binding of rituximab, CD20 was reduced, alkylated, and assayed for rituximab binding. As can be seen in Figure 4, this procedure substantially reduced the ability of rituximab to bind CD20. As an additional control, we reduced CD20, removed the DTT, and allowed the protein to reoxidize under simple air-oxidation conditions. Rituximab binding was partially restored in this procedure, consistent with the

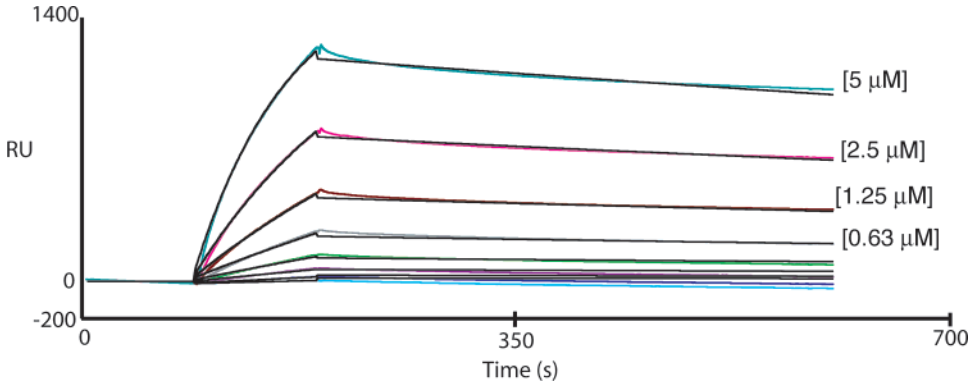

FIGURE 5: Biacore sensograms showing binding of rituximab and human His-tagged CD20. Binding of human CD20 to immobilized rituximab, at CD20 concentrations of 5, 2.5, 1.25, 0.63, 0.31, 0.16, 0.08, and 0.04 μM. Concentrations for the first 4 samples are labeled on the sensogram. The calculated theoretical fits to a noncooperative, monovalent, model are shown in black for each concentration. Full-length rituximab was deposited at 10 000 RU, and human CD20 at the indicated concentrations was applied to the sensor chip at a flow rate of 20 μL/min in 150 mM NaCl, 20 mM HEPES at pH 7.2, and 0.1% DDM.

reformation of the disulfide bond in CD20, thus demonstrating that antibody binding is dependent upon disulfide bond formation. Because antibodies for the extracellular region of murine CD20 are currently unavailable, it was not possible to develop a similar assay for murine CD20.

The ELISA assay of CD20 described above may incorporate avidity effects in the antibody-binding data. To evaluate the binding of rituximab to human CD20 independent of such effects, we utilized surface plasmon resonance. This technique has the added advantage of providing both kinetic binding information and equilibrium binding constants. In these experiments, rituximab or rituximab Fab was deposited on a Biacore sensor chip and soluble human CD20 was passed over the chip at various concentrations. Interestingly, although CD20 could be isolated in DDPC, binding of CD20 to immobilized rituximab was significantly reduced in the presence of this detergent (data not shown). Therefore, affinities from surface plasmon resonance experiments were determined in the presence of DDM. Representative data from these experiments can be seen in Figure 5, and a summary of the results of these experiments are shown in Table 1. Data are representative of multiple experiments. From Table 1, it can be seen that both His-tagged human CD20 and the C2S mutant of human CD20 have approximately the same binding properties with both full-length rituximab antibody and the Fab fragment, indicating that these Cys-to-Ser mutations have no effect on antibody binding, as would be expected from the predicted location of these residues in the intracellular region of the primary structure (see Figure 1). To determine the percentage of CD20 that is present in our preparations with the proper conformation for antibody binding, we further purified the C2S mutant of human CD20 over a rituximab-affinity column. Although the yields were low, the binding data before and after affinity purification are in general agreement, demonstrating that the majority of purified human CD20 is in a conformation capable of binding rituximab. We do observe a modest improvement in antibody binding after affinity purification with immobilized rituximab. This improved affinity may be due to either improved purity of CD20 or removal of inactive CD20 molecules, and this question is currently under investigation. We observed a small difference in affinity of CD20 for full-length antibody relative to the Fab; this slight difference may be accounted for by surface effects because of coupling of the smaller Fab fragment to the sensor chip or to minor changes in the structure of the Fab after removal of the Fc region.

It is possible that any CD20, which is aggregated in the detergent micell may be contributing an avidity effect to the affinity of both IgG and Fab binding. Although the influences of avidity effects are difficult to rule out, we do not feel that they contribute significantly to the binding observed in this assay for two reasons.

First, affinities of the soluble CD20 for intact rituximab IgG or Fab fragment show less than 2-fold differences. Both the IgG and Fab data show excellent agreement to the theoretical fit predicted for monovalent binding. Divergence from theoretical monovalent binding should be particularly evident for the Biacore experiment using rituximab IgG; however, as can be seen in Figure 5, the theoretical monovalent fit and the actual experimental data for CD20 binding to rituximab IgG are in very close agreement. Thus, the soluble CD20 does not appear to be aggregated, and no additional binding modes need to be postulated to account for the experimental data.

Second, the affinity measurements of both the rituximab IgG and Fab fragment, as determined by Biacore, are in close agreement to the affinity measurements of the rituximab Fab fragment determined from Scatchard analysis of binding on normal human B cells. Typical displacement plots of the binding experiments of rituximab IgG and Fab are shown in Figure 7, and the data from different binding experiments with different B-cell donors are summarized in Table 2. As can be seen from these data, a small 3−4-fold difference exists between the monovalent affinity of rituximab Fab for isolated human CD20 as determined by Biacore and the monovalent affinity of rituximab Fab for CD20 expressed on isolated human B cells (190−280 nM affinities in the Biacore experiments versus 50−60 nM affinities from Scatchard analysis). This small difference may represent inherent differences in the assay methods, physical differences in the protein environment, the presence of detergent, or the lack of CD20-binding partners in the isolated material, among other causes. It is interesting to note the large difference between rituximab IgG and Fab binding to B cells. This suggests that avidity effects may play a role in the binding of rituximab to B cells.

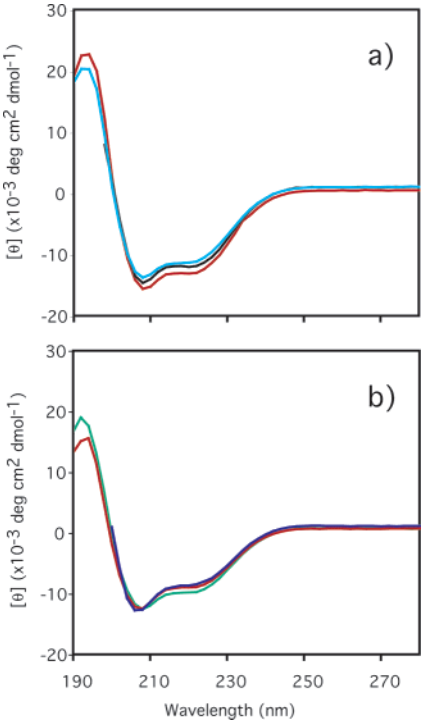

FIGURE 6: Circular dichroic spectra of human and murine CD20. Far-ultraviolet circular dichroic spectra of C2S human CD20 and murine CD20. (a) Human CD20 in the presence of 0.1% DDPC (red), 0.1% DDPC in the presence of 10 mM β-mercaptoethanol (black), and after a thermal scan to 95 °C in the presence of 1% SDS (cyan). (b) Murine CD20 in the presence of 0.1% DDPC (red), 0.1% DDM (green), or 0.1% DDM with the addition of 1% SDS and β-mercaptoethanol after 2 min at 95 °C (navy blue). Data are expressed as molar ellipticities.

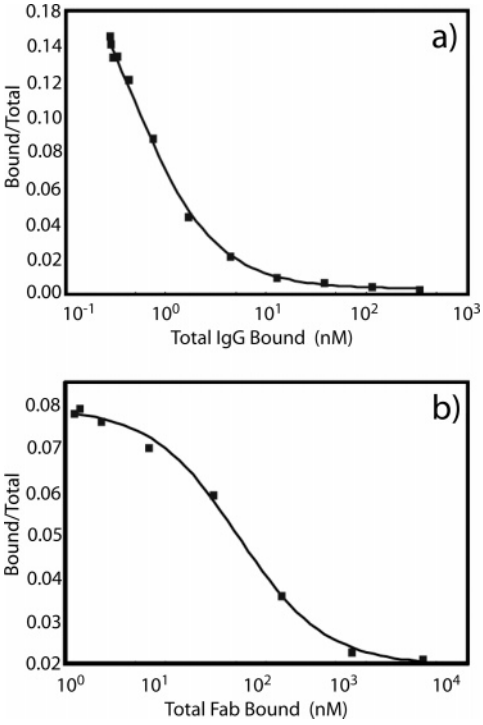

FIGURE 7: Typical displacement plots of rituximab IgG and Fab binding to isolated normal human B cells. Binding was determined by competition of unlabeled rituximab IgG against ^{125}I-IgG for donor 1 (a) or unlabeled rituximab Fab against ^{125}I-Fab for donor 4 (b). See Table 2 for affinities and number of receptors from each donor.

As would be expected from the K_d of rituximab for isolated human CD20 (84−170 nM), the association and dissociation binding rates are relatively rapid, particularly in comparison to high-affinity antibodies such as the affinity-matured anti-VEGF antibody (*30*), which has a K_d of <0.15 nM, a k_{on} of 3.6×10^4 M^{-1} s^{-1}, and a k_{off} of $\leq 0.05 \times 10^{-4}$ s^{-1} at 25 °C. However, because the affinities of rituximab IgG or rituximab Fab fragment as determined by Biacore for isolated CD20 are in close agreement with the rituximab Fab affinity determined from Scatchard analysis on normal B cells, it seems likely that the low monovalent affinity value is realistic and does not result from significant amounts of misfolded or non-native conformations being present in isolated hCD20 preparations.

CD20 was further analyzed for secondary structure by CD spectroscopy. Sample spectra from this analysis are shown in Figure 6. On the basis of the predicted topology of CD20 as a tetra-spanning membrane protein, CD20 should have a helical content of ~35%. It can be seen that both the C2S version of human CD20 and murine CD20 demonstrate a significant signal in the 222 nm region of the spectra as would be expected for proteins with a significant α-helical component (Figure 6).

The addition of the reducing agent did not significantly alter the secondary structure of either murine or human CD20 in either the presence of DDPC or SDS (Figure 6). Further, the secondary structure of CD20 appears to be very stable in a broad variety of detergents and temperatures. CD spectra of human CD20 in the presence of SDS or murine CD20 in the presence SDS and reducing agent, after a thermal scan or brief heating, are almost identical to the spectra of the native proteins (see Figure 6). A temperature scan from 25 to 95 °C does indicate that human CD20 loses approximately 35% of the 222 nm helical signal at 95 °C (data not shown). Although there is no evidence of cooperative unfolding or cooperative refolding, the majority of this signal is recovered when the sample is returned to lower temperatures, at least following brief heating (Figure 6). The small difference in heated and unheated human CD20 samples may indicate that some structure is lost permanently and that, perhaps, the amount of permanently denatured protein may increase with a longer exposure to heat. The observation that the addition of the reducing agent to murine CD20 does not significantly

Table 2: IgG and Fab Binding to Isolated Human B Cells[a]

	Rituximab IgG[b]	
human B cells	rituximab IgG $K_d/10^{-9}$ (M)	number of receptors/cell (10^3)
donor 1	0.32 ± 0.053	160 ± 12
donor 2	0.72 ± 0.21	35 ± 4.8
donor 3	1.27 ± 0.39	45 ± 8.1
	Rituximab Fab[c]	
human B cells	rituximab Fab $K_d/10^{-9}$ (M)	number of receptors/cell (10^3)
donor 4	52 ± 5.1	570 ± 52
donor 5	63 ± 23	230 ± 75

[a] Experiments were performed by competition of unlabeled rituximab IgG or Fab against ^{125}I-IgG or rituxan ^{125}I-Fab bound to CD20 displayed on isolated human B cells. Binding experiments utilized triplicate samples at multiple concentrations of unlabeled protein with cells from a single donor. [b] Summary of results from Scatchard analysis of rituximab IgG binding. [c] Summary of results from Scatchard analysis of rituximab Fab binding.

affect thermal stability of the protein in SDS is interesting. It is possible that the disulfide bond, which is outside the regions of CD20 that are predicted to have α-helical structure, may contribute very little to the overall structural stability of CD20. It is also likely that changes to the structure of CD20 resulting from the reduction of the disulfide bond are simply not observable by CD. It has been previously noted that reduction of the disulfide bond of the β2 adrenergic receptor also had limited effects on the secondary structure as measured by CD (*31*). Similarly, the secondary structure of diacylglycerol kinase is not effected by SDS under conditions similar to those used here (*32*).

On the basis of the antibody-binding properties and secondary structure of the isolated CD20, it is likely that this protein retains a substantially native-like conformation when isolated in detergents, However, more conclusive evidence of the native conformation of CD20 will require determination of the three-dimensional structure of this important B-cell marker.

CONCLUSIONS

We have demonstrated that human CD20 can be expressed in *E. coli*, that this protein co-isolates with bacterial membranes, and that this protein can be purified under nondenaturing conditions. CD spectra of purified human and murine CD20 reveal a protein of substantial helicity as predicted from the primary structure of CD20. Further, the secondary structure of the isolated protein is remarkably resistant to disruption by either detergent or heating. We expect that the availability of recombinant CD20 will aid in research efforts to understand the function of CD20; further experiments to characterize the biophysical and biochemical properties of CD20 are underway in our lab.

The therapeutic antibody rituximab, which recognizes CD20 in a native conformation expressed on B cells, is also capable of recognizing the expressed and purified human CD20 with nanomolar affinity. Additionally, binding of rituximab to CD20 is dependent upon the oxidation state of cysteines in the extracellular domain of the protein, providing some of the first evidence for disulfide bond formation in the extracellular loop of CD20. Inspection of the amino acid sequences of other proteins in the MS4A family reveals that the ability to form a disulfide bond in the loop region between the third and fourth transmembrane segments is a conserved feature in over 50% of the genes in this family (*9*).

Finally, the affinity of rituximab IgG for B cells is shown to be highly dependent upon the ability to bind multiple copies of CD20 on the cell surface. The ability of an IgG antibody to bind bivalently to an antigen expressed on a cell membrane is dependent upon both the expression level of the antigen and steric restrictions imposed by the conformation of the antibody−antigen complex. The bivalent binding of CD20 by rituximab on B cells provides an explanation for the observation that antibodies such as rituximab partition CD20 into lipid rafts, which is correlated with high CDC activity of antibodies (*14*), while other antibodies such as B1, which do not induce CD20 to move into lipid rafts, show little CDC activity (*14*).

ACKNOWLEDGMENT

The authors gratefully acknowledge R. Kelley for help with the Biacore and CD analyses, D. Reilly and E. Missildine for assistance in the large-scale expression of CD20, M. Ultsch for providing the rituximab Fab, A. Namenuk for help with the ELISA, and M. Sliwkowski and D. Dowbenko for helpful discussions.

REFERENCES

1. Stashenko, P., Nadler, L. M., Hardy, R., and Schlossman, S. F. (1980) Characterization of a human B lymphocyte-specific antigen, *J. Immunol. 125*, 1678−1685.
2. Nadler, L. M., Ritz, J., Hardy, R., Pesando, J. M., Schlossman, S. F., and Stashenko, P. (1981) A unique cell surface antigen identifying lymphoid malignancies of B cell origin, *J. Clin. Invest. 67*, 134−140.
3. Einfeld, D. A., Brown, J. P., Valentine, M. A., Clark, E. A., and Ledbetter, J. A. (1988) Molecular cloning of the human B cell CD20 receptor predicts a hydrophobic protein with multiple transmembrane domains, *EMBO J. 7*, 711−717.
4. Leveille, C., Chandad, F., Al-Daccak, R., and Mourad, W. (1999) CD20 is physically and functionally coupled to MHC class II and CD40 on human B cell lines, *Eur. J. Immunol. 29*, 65−74.
5. Szollosi, J., Horejsi, V., Bene, L., Angelisova, P., and Damjanovich, S. (1996) Supramolecular complexes of MHC class I, MHC class II, CD20, and tetraspan molecules (CD53, CD81, and CD82) at the surface of a B cell line JY, *J. Immunol. 157*, 2939−2946.
6. Kansas, G. S., and Tedder, T. F. (1991) Transmembrane signals generated through MHC class II, CD19, CD20, CD39, and CD40 antigens induce LFA-1-dependent and independent adhesion in human B cells through a tyrosine kinase-dependent pathway, *J. Immunol. 147*, 4094−4102.
7. Adra, C. N., Lelias, J. M., Kobayashi, H., Kaghad, M., Morrison, P., Rowley, J. D., and Lim, B. (1994) Cloning of the cDNA for a hematopoietic cell-specific protein related to CD20 and the β subunit of the high-affinity IgE receptor: Evidence for a family of proteins with four membrane-spanning regions, *Proc. Natl. Acad. Sci. U.S.A. 91*, 10178−10182.
8. Ishibashi, K., Suzuki, M., Sasaki, S., and Imai, M. (2001) Identification of a new multigene four-transmembrane family (MS4A) related to CD20, HTm4, and β subunit of the high-affinity IgE receptor, *Gene 264*, 87−93.
9. Liang, Y., and Tedder, T. F. (2001) Identification of a CD20-, FcϵRIβ-, and HTm4-related gene family: Sixteen new MS4A family members expressed in human and mouse, *Genomics 72*, 119−127.
10. Tedder, T. F., and Engel, P. (1994) CD20: A regulator of cell-cycle progression of B lymphocytes, *Immunol. Today 15*, 450−454.
11. Riley, J. K., and Sliwkowski, M. X. (2000) CD20: A gene in search of a function, *Semin. Oncol. 27*, 17−24.
12. Berinstein, N. L., Grillo-Lopez, A. J., White, C. A., Bence-Bruckler, I., Maloney, D., Czuczman, M., Green, D., Rosenberg, J., McLaughlin, P., and Shen, D. (1998) Association of serum rituximab (IDEC-C2B8) concentration and anti-tumor response in the treatment of recurrent low-grade or follicular non-Hodgkin's lymphoma, *Ann. Oncol. 9*, 995−1001.
13. Deans, J. P., Robbins, S. M., Polyak, M. J., and Savage, J. A. (1998) Rapid redistribution of CD20 to a low-density detergent-insoluble membrane compartment, *J. Biol. Chem. 273*, 344−348.
14. Cragg, M. S., Morgan, S. M., Chan, H. T., Morgan, B. P., Filatov, A. V., Johnson, P. W., French, R. R., and Glennie, M. J. (2003) Complement-mediated lysis by anti-CD20 mAb correlates with segregation into lipid rafts, *Blood 101*, 1045−1052.
15. Polyak, M. J., Tailor, S. H., and Deans, J. P. (1998) Identification of a cytoplasmic region of CD20 required for its redistribution to a detergent-insoluble membrane compartment, *J. Immunol. 161*, 3242−3248.
16. Bubien, J. K., Zhou, L. J., Bell, P. D., Frizzell, R. A., and Tedder, T. F. (1993) Transfection of the CD20 cell surface molecule into ectopic cell types generates a Ca^{2+} conductance found constitutively in B lymphocytes, *J. Cell. Biol. 121*, 1121−1132.
17. Li, H., Ayer, L. M., Lytton, J., and Deans, J. P. (2003) Store-operated cation entry mediated by CD20 in membrane rafts, *J. Biol. Chem. 278*, 42427−42434.
18. Ausubel, F. M., Brent, R., Kingston, R. E., Moore, D. D., Seidman, J. G., Smith, J. A., and Struhl, K. (2003) John Wiley and Sons, New York.
19. Simmons, L. C., Reilly, D., Klimowski, L., Raju, T. S., Meng, G., Sims, P., Hong, K., Shields, R. L., Damico, L. A., Rancatore,

P., and Yansura, D. G. (2002) Expression of full-length immunoglobulins in *Escherichia coli*: Rapid and efficient production of aglycosylated antibodies, *J. Immunol. Methods 263*, 133−147.

20. Smith, P. K., Krohn, R. I., Hermanson, G. T., Mallia, A. K., Gartner, F. H., Provenzano, M. D., Fujimoto, E. K., Goeke, N. M., Olson, B. J., and Klenk, D. C. (1985) Measurement of protein using bicinchoninic acid, *Anal. Biochem. 150*, 76−85.
21. Munson, P. J., and Rodbard, D. (1980) Ligand: A versatile computerized approach for characterization of ligand-binding systems, *Anal. Biochem. 107*, 220−239.
22. McPherson, G. A. (1983) A practical computer-based approach to the analysis of radioligand binding experiments, *Comput. Programs Biomed. 17*, 107−113.
23. Valentine, M. A., Meier, K. E., Rossie, S., and Clark, E. A. (1989) Phosphorylation of the CD20 phosphoprotein in resting B lymphocytes. Regulation by protein kinase C, *J. Biol. Chem. 264*, 11282−11287.
24. Tedder, T. F., and Schlossman, S. F. (1988) Phosphorylation of the B1 (CD20) molecule by normal and malignant human B lymphocytes, *J. Biol. Chem. 263*, 10009−10015.
25. Creighton, T. E. (1993) *Proteins Structures and Molecular Properties*, 2 ed., W. H. Freeman and Company, New York.
26. Ishidate, K., Creeger, E. S., Zrike, J., Deb, S., Glauner, B., MacAlister, T. J., and Rothfield, L. I. (1986) Isolation of differentiated membrane domains from *Escherichia coli* and *Salmonella typhimurium*, including a fraction containing attachment sites between the inner and outer membranes and the murein skeleton of the cell envelope, *J. Biol. Chem. 261*, 428−443.
27. Bertin, B., Freissmuth, M., Breyer, R. M., Schutz, W., Strosberg, A. D., and Marullo, S. (1992) Functional expression of the human serotonin 5-HT1A receptor in *Escherichia coli*. Ligand binding properties and interaction with recombinant G protein α-subunits, *J. Biol. Chem. 267*, 8200−8206.
28. Grisshammer, R., Duckworth, R., and Henderson, R. (1993) Expression of a rat neurotensin receptor in *Escherichia coli*, *Biochem. J. 295* (part 2), 571−576.
29. Polyak, M. J., and Deans, J. P. (2002) Alanine-170 and proline-172 are critical determinants for extracellular CD20 epitopes; heterogeneity in the fine specificity of CD20 monoclonal antibodies is defined by additional requirements imposed by both amino acid sequence and quaternary structure, *Blood 99*, 3256−3262.
30. Chen, Y., Wiesmann, C., Fuh, G., Li, B., Christinger, H. W., McKay, P., de Vos, A. M., and Lowman, H. B. (1999) Selection and analysis of an optimized anti-VEGF antibody: Crystal structure of an affinity-matured Fab in complex with antigen, *J. Mol. Biol. 293*, 865−881.
31. Lin, S., Gether, U., and Kobilka, B. K. (1996) Ligand stabilization of the β 2 adrenergic receptor: Effect of DTT on receptor conformation monitored by circular dichroism and fluorescence spectroscopy, *Biochemistry 35*, 14445−14451.
32. Lau, F. W., and Bowie, J. U. (1997) A method for assessing the stability of a membrane protein, *Biochemistry 36*, 5884−5892.

BI0511078